

FIVE NEW FAINT CATAclySMIC VARIABLES FROM THE ZWICKY TRANSIENT FACILITY

CHRISTOPHER LLOYD¹ AND KLAUS BERNHARD²

1) Department of Physics and Astronomy, University of Sussex, Brighton, BN1 9QH C.Lloyd@sussex.ac.uk

2) Bundesdeutsche Arbeitsgemeinschaft für Veränderliche Sterne e.V. (BAV), Munsterdamm 90, D-12169 Berlin
klaus.bernhard@liwest.at

Abstract: A search of faint, large-amplitude variables in the Zwicky Transient Facility data has led to the identification of five new CVs. Four of the stars, ZTFJ010013.34+610809.8, ZTFJ051913.86+293006.0, ZTFJ210441.02+394052.7 and ZTFJ210705.14+394617.7 are probably SS Cyg-type systems, while ZTFJ173854.93+175136.3 is a likely SU UMa system.

1 Introduction

Cataclysmic variables (CVs) are interacting binary systems which comprise a low-mass secondary star (mostly a red dwarf) losing material to a white dwarf primary star. They exhibit complex photometric variability, which is characterised by a variety of phenomena, most notably abrupt and conspicuous brightenings (*i.e.*, dwarf nova outbursts, nova eruptions or supernovae) but also orbital modulation, eclipses, flickering, and long term variations.

Dwarf novae or U Geminorum variables (UG) form a major division of CVs distinct from supernovae, novae and nova-like variables (which do not show UG-type outbursts), and similar systems with strong magnetic fields. Nevertheless, many low-amplitude eruptive-like variables are initially classified as UG on the basis of limited photometry. Outbursts of U Gem variables are typically 2–6 or even 8 magnitudes in *V*, rising in 1–2 days and returning to their original brightness over several subsequent days. The interval between outbursts ranges from ~ 10 to hundreds of days, or years for some systems. Three main classifications of U Gem variables are recognised and these are based on the prototype light curves of SS Cygni (UGSS), Z Camelopardalis (UGZ) and SU Ursae Majoris (UGSU), but there are many subclasses and these are described in detail on the [VSX variability types page](#) (see also Kato et al. (2012); Coppejans et al. (2016) for a more general description). SS Cyg-type stars usually show well-separated outbursts of broadly equal amplitude, with limited variation at quiescence, although there is considerable variety between systems and also some change in behaviour over time in the same system (see *e.g.*, Price et al., 2007). Z Cam-type stars tend to show more regular outbursts but are characterised by standstills in the light curve and the behaviour before and after the standstill is frequently different. See Simonsen et al. (2014) for a review of the light curves of these systems. By contrast, SU UMa-type systems show two types of outburst. The normal outbursts are short lived but frequent, and these are interspersed with occasional brighter and longer superoutbursts, which are characterised by a near-orbital modulation termed

superhumps (see *e.g.*, Osaki & Kato, 2013; Kato et al., 2020). While the definitive classification of some UG subtypes requires detailed time-series photometry or spectroscopy it remains the case that a good initial classification can be made from a reasonably well sampled light curve. However, the other side of that coin is that the characteristics of the light curves can change, and when studied in detail systems can show features of more than one subtype. They are complex variables. For a general review of CVs see Warner (1995) and Hellier (2001).

2 Observations and analysis

The observations are taken from the Zwicky Transient Facility (ZTF) sky survey situated at Palomar Observatory. Taking up the legacy of its predecessor, the Palomar Transient Factory, it has been observing the available northern sky since 2018. The ZTF camera employs e2v CCD231-C6 devices and is mounted on the Palomar 48-inch Samuel Oschin Schmidt Telescope. High-quality data are collected in g and r , and occasionally in i , as other programmes permit, down to a limiting magnitude of $r \sim 20.6$, and made publicly available through the [IPAC archive](#)¹ (Bellm et al., 2019a,b; Masci et al., 2019).

Chen et al. (2020) exploited ZTF Data Release 2 and compiled a catalogue of $\sim 780\,000$ periodic variable stars (The Zwicky Transient Facility Catalog of Periodic Variable Stars) and $\sim 1\,000\,000$ suspected variables ([The ZTF Suspected Variables Catalog](#)²). Of course, these two catalogues do not contain a category for rare objects like cataclysmic variables so it is assumed that any such objects will have been assigned to the ZTF Suspected Variables Catalog because of their rather complex variability pattern consisting of large amplitude variations and considerable changes of the light curve shape. The ZTF Suspected Variables Catalog was systematically searched for cataclysmic variables by visually inspecting the light curves of an extended sample of stars with amplitudes of more than 2 magnitudes in the g band. This search led to the discovery of the five CVs discussed here. At that time none of these objects were classified in the SAO/NASA Astrophysics Data System or the AAVSO’s International Variable Star Index (VSX), however, since then one of the stars, ZTFJ051913.86+293006.0 = ZTF17aacayci has been independently identified as a likely CV by Förster et al. (2021).

ZTF data are available from early in 2018 so depending on the visibility of the object there will be up to four complete observing seasons, although the coverage is not even and tends to be lower in recent years. The cadence of the data is also irregular with some almost contiguous runs over several nights and some unfortunately large gaps during the observing season. For the systems discussed here there are typically 600–700 observations split between g and r in the ratio of about 3:4, with a small number of i observations, between zero and 50. The occurrence of observations in different bands is correlated to some extent and these data, taken within 0^h5 comprise about 25% of the total, and are used to measure the $(g - r)$, and $(r - i)$ colours when possible.

The light curves had been used to provide the maximum and minimum magnitudes and the $(g - r)$ and $(r - i)$ colours. The magnitudes at maximum and minimum brightness

¹IPAC archive - <https://irsa.ipac.caltech.edu/Missions/ztf.html>

²The ZTF Suspected Variables Catalog - doi.org/10.5281/zenodo.3886372

Table 1: Basic identification and photometric data

Name	RA	Dec	max	min	range
ZTF			g	g	Δg
Gaia EDR3			r	r	Δr
			$(g - r)$	$(g - r)$	$\Delta(g - r)$
			mean $(r - i)$		
ZTFJ010013.34+610809.8	01 00 13.360	+61 08 09.86	18.8	21.5	2.7
426610064901005184			17.9	20.5	2.6
			1.11	1.05	-0.06
			0.52		
ZTFJ051913.86+293006.0	05 19 13.871	+29 30 05.98	18.4	20.8	2.4
3446482973237446272			17.7	19.6	1.9
			0.63	1.02	0.39
			–		
ZTFJ173854.93+175136.3	17 38 54.935	+17 51 36.08	19.7	21.7	2.1
4550394709106157184			19.8	21.4	1.6
			-0.01	0.14	0.14
			0.15		
ZTFJ210441.02+394052.7	21 04 41.022	+39 40 52.68	18.5	20.7	2.2
1872331554654601472			17.8	19.4	1.6
			0.82	1.23	0.41
			0.47		
ZTFJ210705.14+394617.7	21 07 05.151	+39 46 17.69	18.8	21.7	2.9
1872300660944066560			18.5	20.5	2.0
			0.64	1.03	0.39
			0.59		

are taken to be the 5 and 95 percentiles of the daily ZTF magnitudes in g and r . These measures are used to provide consistent and impartial values of some mean maximum and minimum brightness, but these will not necessarily align with any obvious feature of the light curve. The measured magnitude at maximum is typically $0^m.5$ fainter than the brightest magnitudes seen. At maximum the photometric errors are $< 0^m.05$ so are trivial compared with the variations in the light curve. At minimum the measured magnitude is $\sim 0^m.5$ brighter than the faintest magnitudes, but this depends on the distribution of the data at minimum. The uncertainties at minimum are $\sim 0^m.2$ in g and r so the measured minimum magnitude is typically $2\text{--}3\sigma$ above the faintest magnitude and robust against photometric errors. Typically this value lies near the faint edge of the bulk of the points near quiescence, but for systems that spend little time at quiescence the value does not correspond to any obvious feature in the light curve. The $(g - r)$ values are derived from contemporaneous g and r magnitudes, and are given for the brighter and fainter halves of the data. The distribution of $(g - r)$ shows considerable scatter but the standard error of the mean is $< 0^m.03$, depending on the statistics. Changes in $|g - r| > 0.1$ are very significant and the gradient of $\Delta(g - r)/\Delta r$ has also been used to test this change. The mean $(r - i)$ is also listed but only the last two systems have more than a handful of i

observations.

Data have also been taken from the Pan-STARRS DR1 survey (Chambers et al., 2016) which provided about 50 observations between 2009–2014 for each of the objects. These are divided almost equally between the g , r , i , z , and y bands, although for some systems not all bands are present. The data are very sparse but do provide a snapshot of the activity at a different epoch to the ZTF data.

3 Results

The basic identification and photometric details of the five systems are given in Table 1. The ZTF identifier from Chen et al. (2020) and the *Gaia* EDR3 identifier are given together with the EDR3-based position from Simbad. The magnitudes at maximum and minimum brightness in g and r , and the range in both bands is listed. The $(g - r)$ for the brighter and fainter halves of the r data are also given, together with the range in this colour, and the mean $(r - i)$ as available.

3.1 ZTFJ010013.34+610809.8

ZTFJ010013.34+610809.8 has mean $G = 20.2$ and has a marginally brighter companion at 5.7 arcsec. ZTF observations are available for four almost complete observing seasons from 2018 – 2021. There are only three i observations. The epoch plot (see Figure 1) shows about six outbursts per season with amplitudes of 2–3 magnitudes in both g and

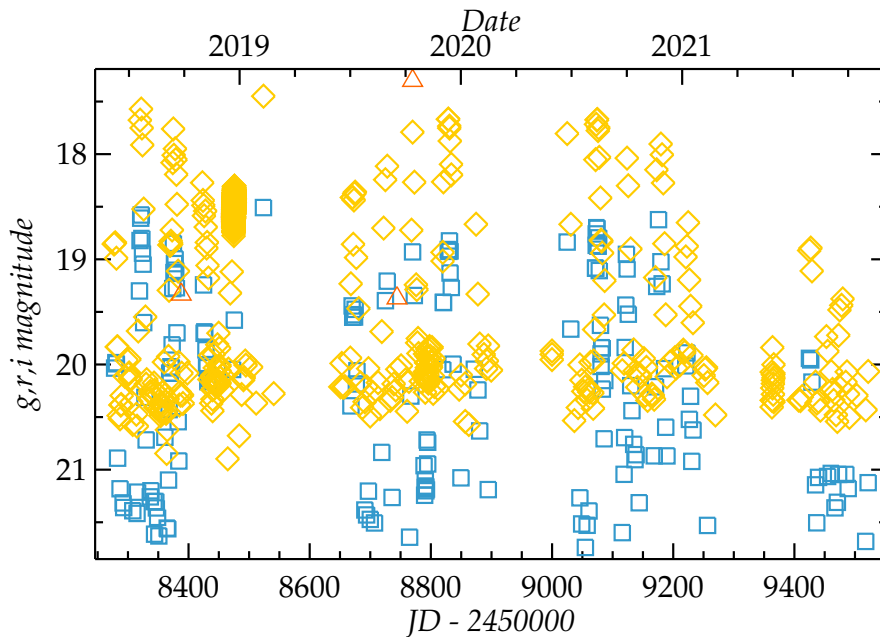


Figure 1: Epoch plot of ZTFJ010013.34+610809.8 from the 2018 observing season to the present showing the ZTF g (squares), r (diamonds) and i -band data (triangles). Several outbursts are clearly visible and even at this scale they appear remarkably clean with little activity near quiescence.

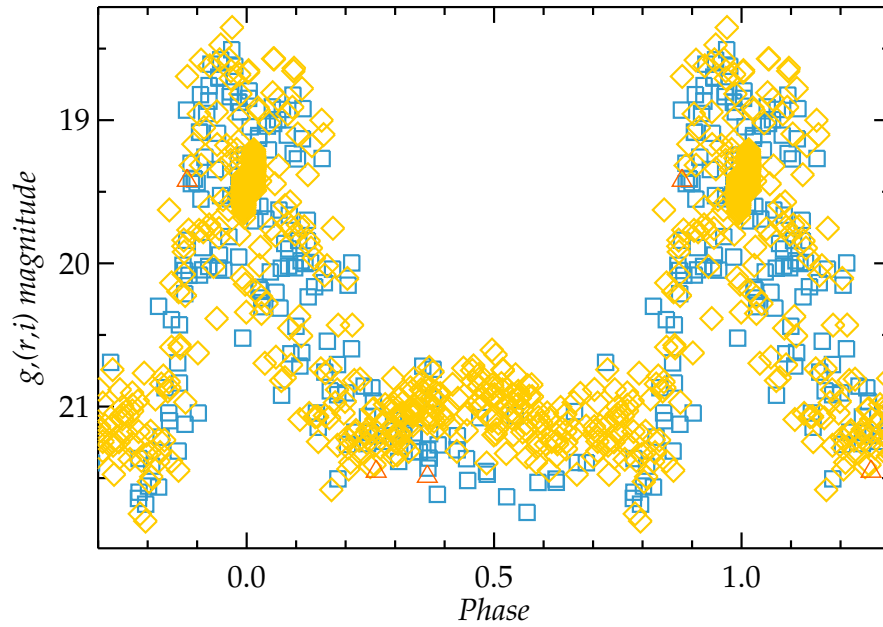


Figure 2: Phase plot of the ZTFJ010013.34+610809.8 data folded on a period of 50.1 days. The main outburst is clearly resolved in both the g (squares) and r data (diamonds), and a low-amplitude intermediate outburst is also visible in the r data.

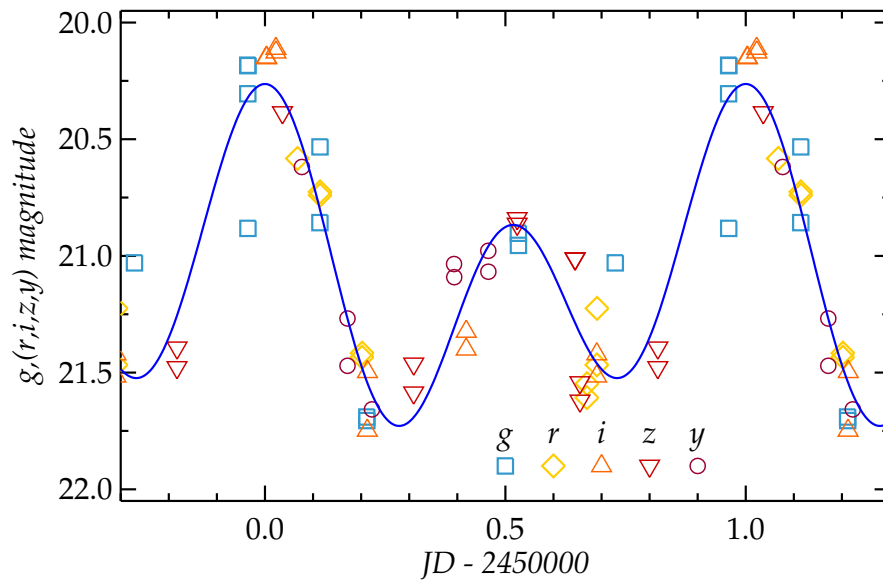


Figure 3: Phase plot of the Pan-STARRS data of ZTFJ010013.34+610809.8 data folded on a period of 50.1 days with the two-harmonic Fourier fit superimposed. The different bands have been allowed to float in the fit and are aligned on the g -band data. Although the data are sparse the main outburst is clearly resolved and a low-amplitude intermediate outburst is also visible. The symbols used here are the same as in the other ZTF and Pan-STARRS plots.

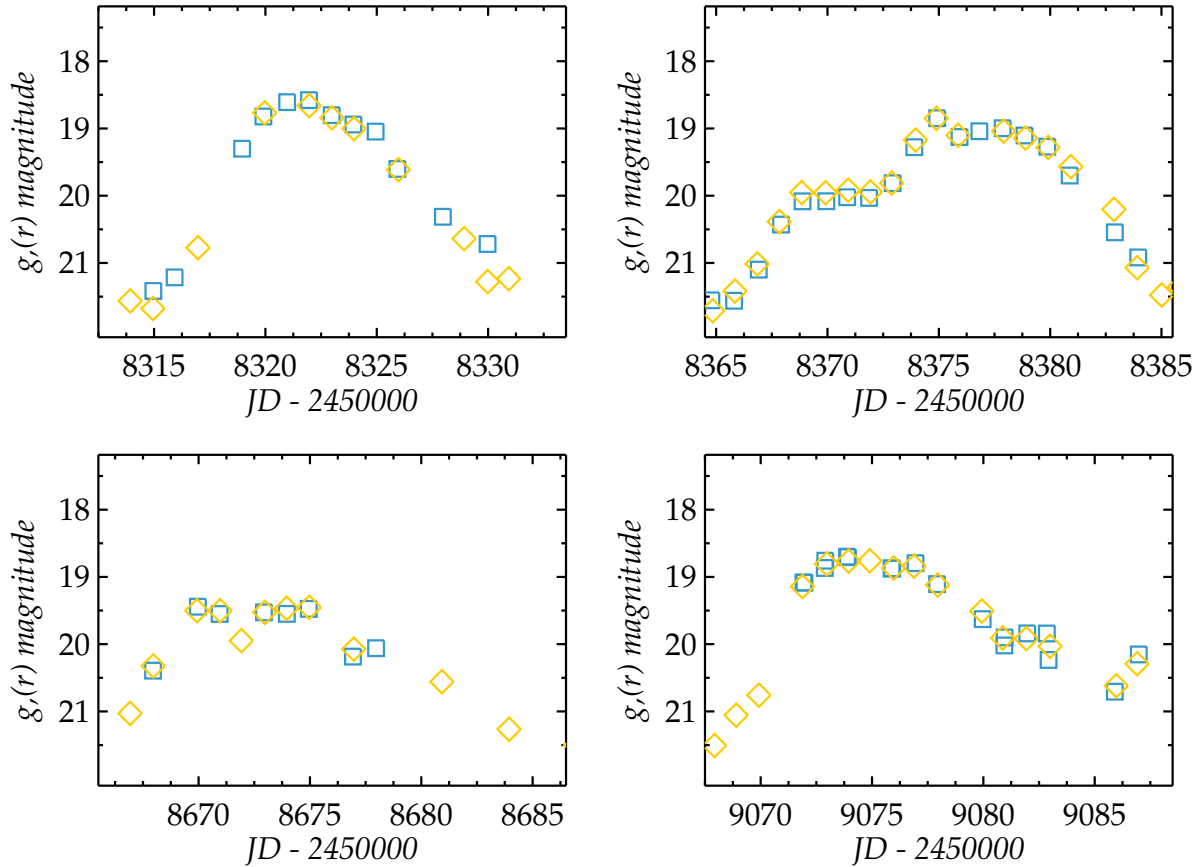


Figure 4: Epoch plots each covering about 20 days around four of the best observed outbursts of ZTFJ010013.34+610809.8 with the r -band data (diamonds) aligned on the g data (squares) using the bright $(g-r)$ offset in Table 1. These outbursts were chosen to illustrate the variation in brightness and profile of the main outburst.

r for the first three seasons, but the coverage, and possibly the activity, is lower in the last season. The spacing between the outbursts appears relatively constant and this is confirmed by a power spectrum of the data which shows a clear single peak near 50 days. The individual g , r , and combined data sets were fitted with a two-harmonic Fourier series with the different data bands allowed to float in the combined fit, and the best period was found to be 50.1 ± 1.0 for all sets. The data folded on this period are shown in Figure 2. The main peak is clearly resolved and there appears to be a much weaker secondary peak in the r data. The g data at this phase are more sparse and scattered so this secondary feature is less visible, and less consistent, but the g and r data may be less correlated.

The Pan-STARRS DR1 data (Chambers et al., 2016) data have also been fitted with a two-harmonic Fourier series with the different data bands allowed to float, and the best period was again found to be 50.1 ± 2.5 days. The phase diagram of the Pan-STARRS data folded on this period is shown in Figure 3. Although the general behaviour over the two data sets is remarkably similar the amplitude of the outburst appears lower in the Pan-STARRS data, but the ZTF data show a large degree of variation and the 2021

season may show generally lower activity.

The light curve is characteristic of a SS Cyg-type system although these show an enormous range of behaviour between systems, and over time in the same system. One pattern of behaviour shows alternating stronger and weaker outbursts, and that appears to be the case here, although it is particularly extreme. There is also usually significant variation in the outburst timings that destroys any coherence over time, so again, the regularity seen here is unusual.

The range in g and r is essentially identical and although $(g - r)$ is marginally bluer at minimum, this is not significant from the colours nor from the gradient of $\Delta(g - r)/\Delta r$. The small difference in range for different bands probably persists through the Pan-STARRS data as they are generally consistent in Figure 3.

Detailed plots of the best observed individual outbursts are given in Figure 4 and these clearly show the variation in outburst profile, timing and amplitude. Each panel shows about 20 days and the r data have been aligned on the g data using the bright $(g - r)$ offset in Table 1 so the peaks of the outbursts are better defined.

3.2 ZTFJ051913.86+293006.0 = ZTF17aacayci

ZTFJ051913.86+293006.0 has $G = 19.5$ and a companion 1^m4 brighter at 6.1 arcsec. The light curve of the ZTF data (see Figure 5) shows sixteen outbursts with $g < 19.0$ between 2018 and 2021 with amplitudes of 2–3 magnitudes. There are a few fainter, partially observed outbursts but the activity around quiescence is limited to $\sim 0^m5$ with no sign of

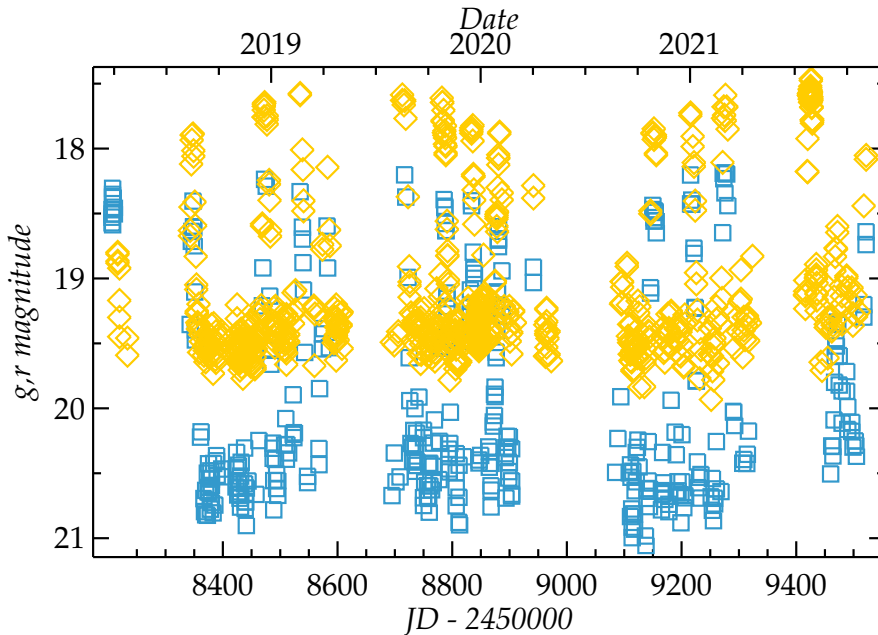


Figure 5: Epoch plot of ZTFJ051913.86+293006.0 from 2018 to the present showing the ZTF g (squares) and r -band data (diamonds). Fourteen outbursts are clearly visible with no intermediate outbursts and little activity near quiescence.

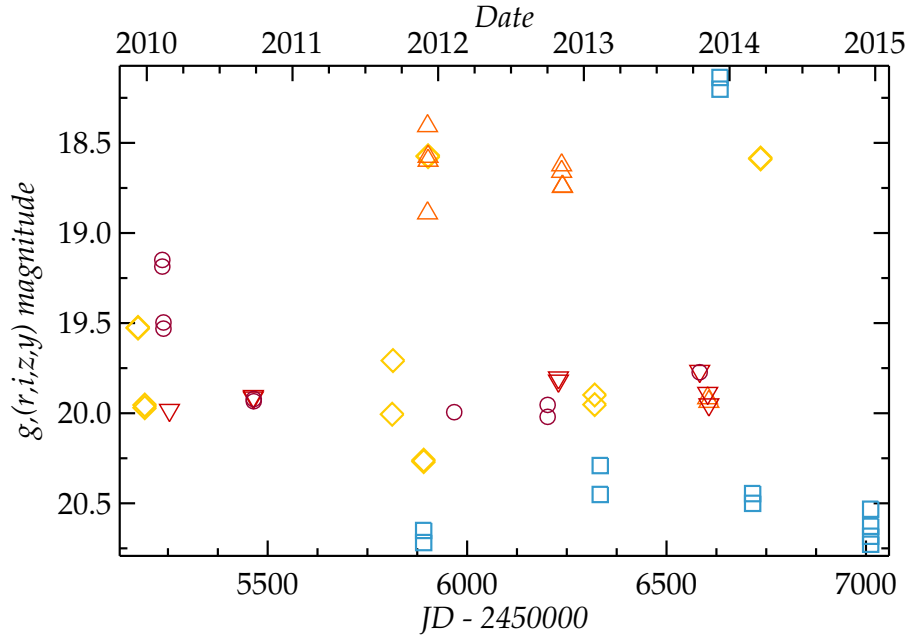


Figure 6: Epoch plot of the Pan-STARRS data of ZTFJ051913.86+293006.0 data from 2009–2014 with the different bands aligned on the g data based on the ZTF colours from Table 1 and those derived from a small number of contemporaneous Pan-STARRS observation in different bands. The symbols are as in Figure 3. The range in g is comparable to the ZTF data so the behaviour is probably similar at both epochs.

intermediate, fainter outbursts.

The Pan-STARRS data are shown in Figure 6 with the different bands aligned on the g data based on the ZTF ($g - r$) and when available ($r - i$) colours, and those derived from a small number of contemporaneous Pan-STARRS observation in different bands. Despite the sparse coverage the range in g is similar to the ZTF data so the behaviour at this earlier epoch is probably similar.

Given the high outburst rate and the density of coverage it is possible to estimate the characteristic outburst interval from a histogram of the difference in the outburst timings, as shown in Figure 7. There are seasonal gaps in the data of typically 100 days and other, shorter gaps where outbursts could be missed, but even so there are enough to make a reliable estimate. The minimum outburst interval is 45 days so any intervals longer than twice this are likely to be multiples. There is a natural gap in the histogram at ~ 80 days with two slightly longer intervals at 88 and 103 days, but both of these have intermediate weak or incomplete outbursts so these are apparently multiples. The longer intervals are all most likely multiples. The mean has been determined from intervals < 80 days, which are distributed with a mean of 58 ± 9 days. Given the similar outburst time scale and pattern, and the lack of intermediate outbursts the star is most likely an SS Cyg-type system.

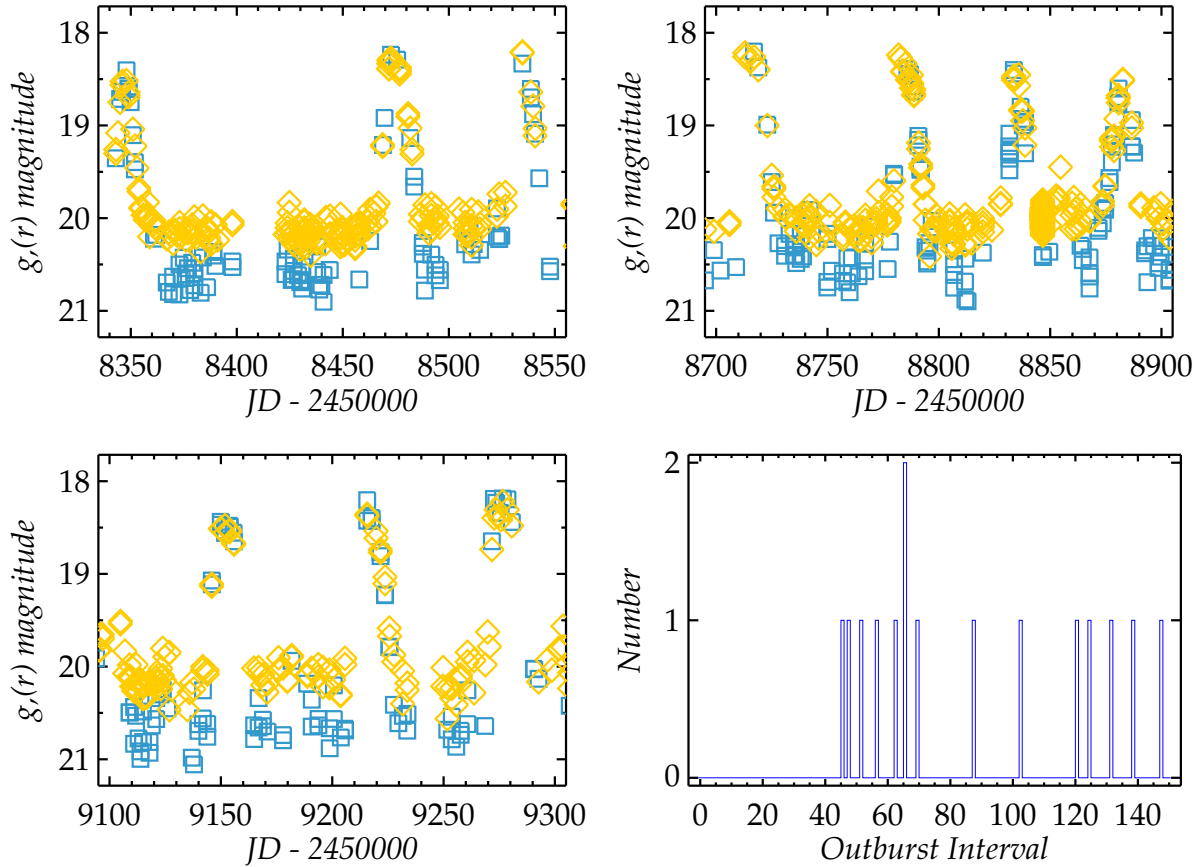


Figure 7: Three panels show detail of the best coverage over about 200 days each for three observing seasons of ZTFJ051913.86+293006.0. The r -band data (diamonds) are aligned on the g magnitudes (squares) using the bright ($g - r$) offset in Table 1. The variation in outburst amplitude and timing is clear, as is the lack of any intermediate outbursts, and the obvious difference in ($g - r$) at quiescence. The fourth panel shows the histogram of the outburst intervals under 150 days. The mean outburst interval has been determined from those < 80 days, where there seems to be a natural divide in the distribution, and corresponds to twice the minimum interval.

3.3 ZTFJ173854.93+175136.3

ZTFJ173854.93+175136.3 has $G = 20.0$ and is positionally coincident with a GALEX source with magnitude $NUV = 21.9 \pm 0.5$ (Bianchi et al., 2011). The ZTF data are available for four complete seasons although coverage in the last two was less dense. The ZTF light curve is shown in Figure 8 and is one of almost continuous activity with myriad outbursts of ~ 2 magnitudes. The outburst frequency is high with the minimum outburst interval in the region of 16–20 days, and the system appears to move from one outburst to the next with little time spent at quiescence. The Pan-STARRS data are shown in Figure 9 and although these are very sparse they also suggest a high level of activity.

Although numerous outbursts can be identified in the ZTF data few of them are covered sufficiently well to provide a good description of the profile. Based on fragmentary data

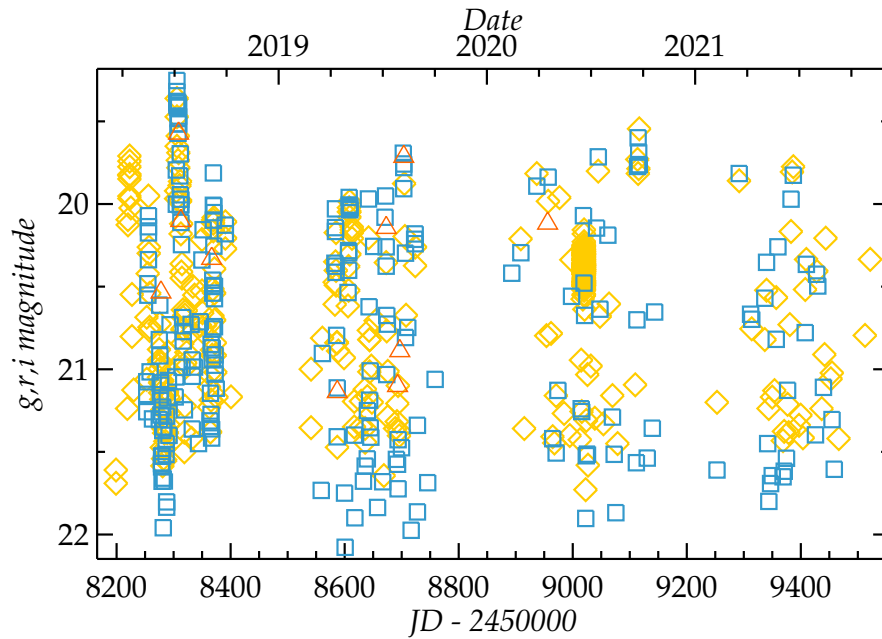


Figure 8: Epoch plot of ZTFJ173854.93+175136.3 from the 2018 observing season to the present showing the ZTF g (squares), r (diamonds) and i -band data (triangles). The system appears to be in a state of near continuous variation and spends little time in quiescence.

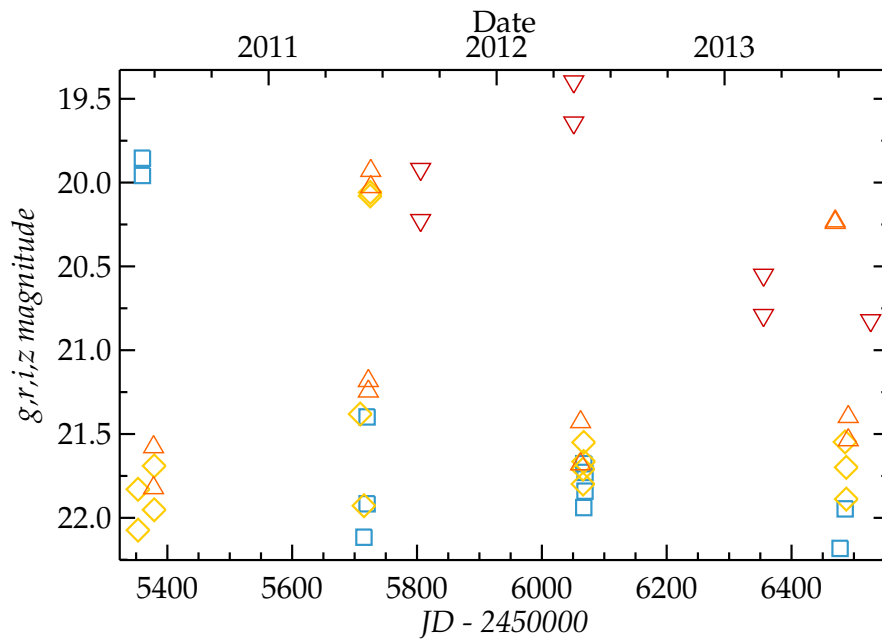


Figure 9: Epoch plot of the Pan-STARRS data of ZTFJ173854.93+175136.3 data with no adjustment to the different bands. Although the data are sparse the rapid variability of the system is clear. The symbols are as in Figure 3.

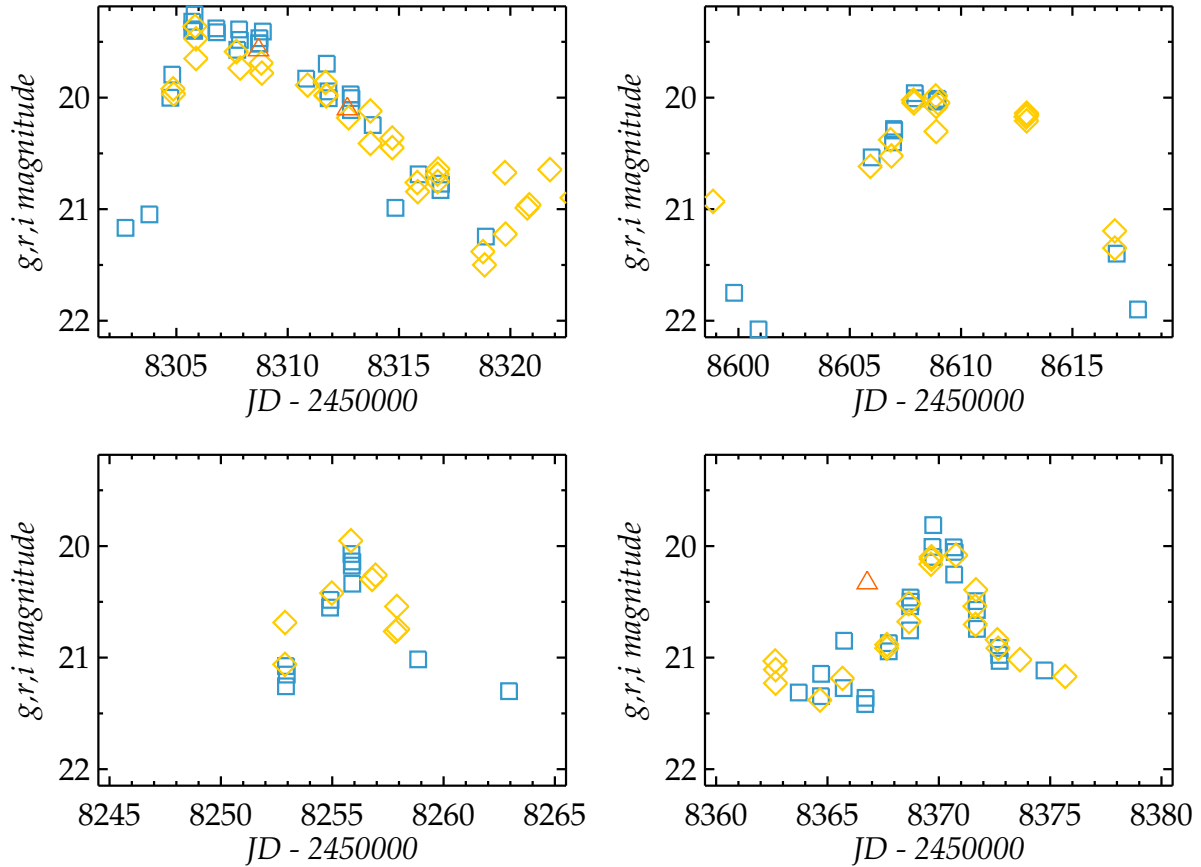


Figure 10: The detail of four individual outbursts of ZTFJ173854.93+175136.3 each covering about 20 days. No offsets have been applied to the r and i magnitudes as the colours are small (see Table 1). The top two panels show the best observed outburst, which is interpreted as a superoutburst, and a second possible superoutburst, although coverage is much less complete. The two bottom panels show the two best defined normal outbursts. The symbols are g (squares), r (diamonds) and i -band data (triangles).

the outbursts seem to divide into two groups. The majority are short duration, ~ 5 days, but a small number are longer at perhaps 12 days, and one of these is the brighter and best covered outburst. Otherwise these longer outbursts are not obviously brighter than the others but this pattern of behaviour suggests that the system is an SU UMa type. Details of four outbursts are shown in Figure 10. Two are suggested as likely superoutbursts and two shorter, possibly weaker ones are probably normal outbursts. The features identified as possible superoutbursts recur on a time scale of about 100 days.

3.4 ZTFJ210441.02+394052.7

ZTFJ210441.02+394052.7 has been observed for four complete observing seasons but the coverage in the most recent one is less dense. The data are slightly different to the other systems discussed here in that there are a substantial number of i -band observations. The system has $G = 19.2$ and a companion 1^m0 fainter at 3.3 arcsec, but there is no

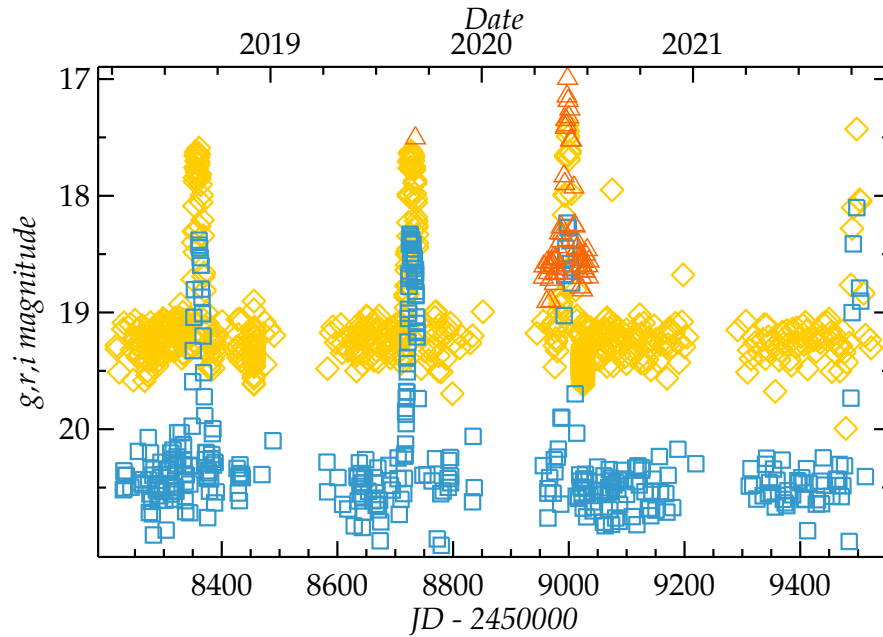


Figure 11: Epoch plot of ZTFJ210441.02+394052.7 from the 2018 observing season to the present showing the ZTF g (squares), r (diamonds) and i -band data (triangles). Four outbursts are clearly visible with no intermediate outbursts and little activity near quiescence.

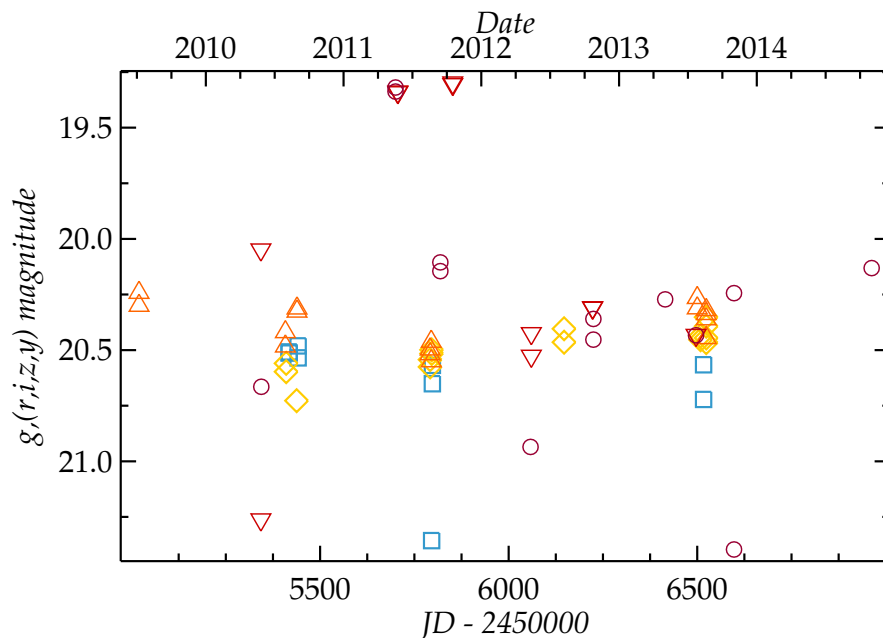


Figure 12: Epoch plot of the Pan-STARRS data of ZTFJ210441.02+394052.7 data with the different bands aligned on the g data based on the contemporaneous ZTF and Pan-STARRS colours. Most of the data are faint, consistent with being in quiescence and the low outburst rate, while the brighter observations are probably two outbursts. The symbols are as in Figure 3.

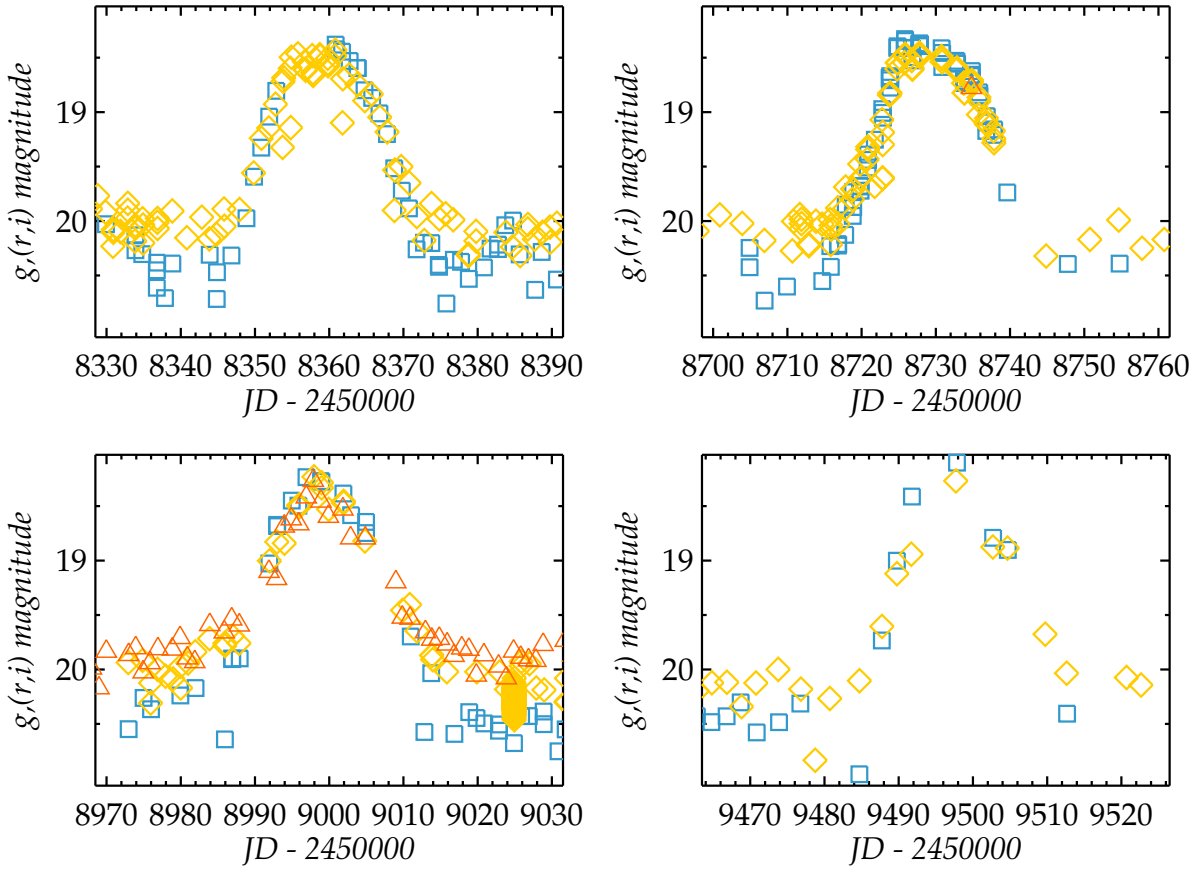


Figure 13: Detail of the ZTFJ210441.02+394052.7 light curve. Four panels showing about 60 days around each of the outbursts visible in Figure 11. The r (diamonds) and i -band data (triangles) are aligned on the g magnitudes (squares) using the bright ($g - r$) offset in Table 1 and the mean ($r - i$) offset.

confusion in the ZTF data. The light curve is shown in Figure 11 and has just four outbursts with amplitudes ~ 2 magnitudes in g and r . Between the outbursts there is very little activity which is limited to $\sim 0^m.5$ with no sign of any intermediate, fainter outbursts. The outbursts have spacings of 371, 268 and 500 days respectively, but it is possible that one or more may have been missed in the seasonal gaps. From the long runs without outbursts in the last two seasons the minimum interval must be > 200 days. The Pan-STARRS data shown in Figure 12 are mostly below $g = 20$ so are consistent with the system being at quiescence, and the few brighter observations have probably caught two of the comparatively rare outbursts. Details of the individual outbursts are shown in Figure 13 and for the most part they have a rather sinusoidal shape. Although the outburst interval is relatively long the pattern of behaviour suggests the system is an SS Cyg-type.

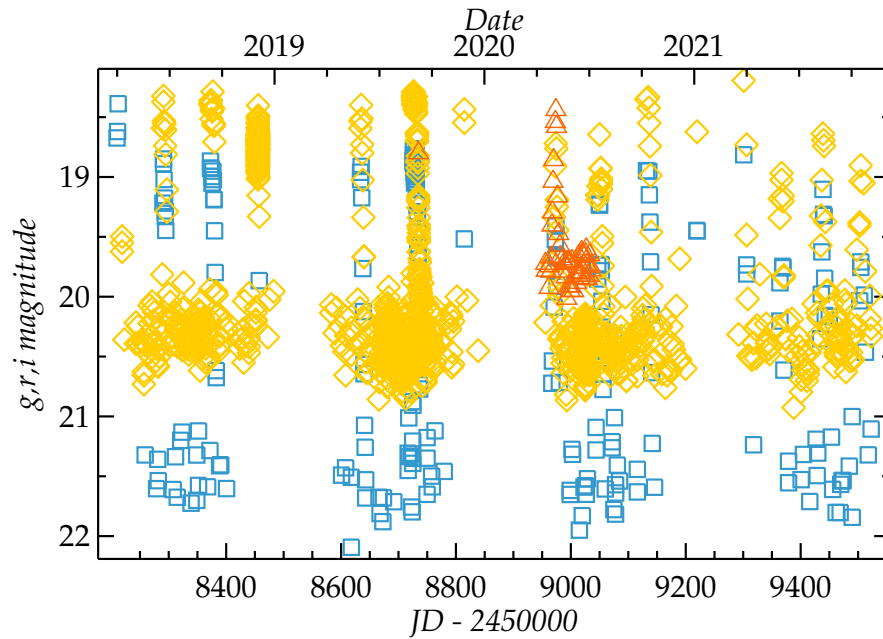


Figure 14: Epoch plot of ZTFJ210705.14+394617.7 from the 2018 observing season to the present showing the ZTF g (squares), r (diamonds) and i -band data (triangles). Fifteen outbursts are clearly visible with no intermediate outbursts and little activity near quiescence.

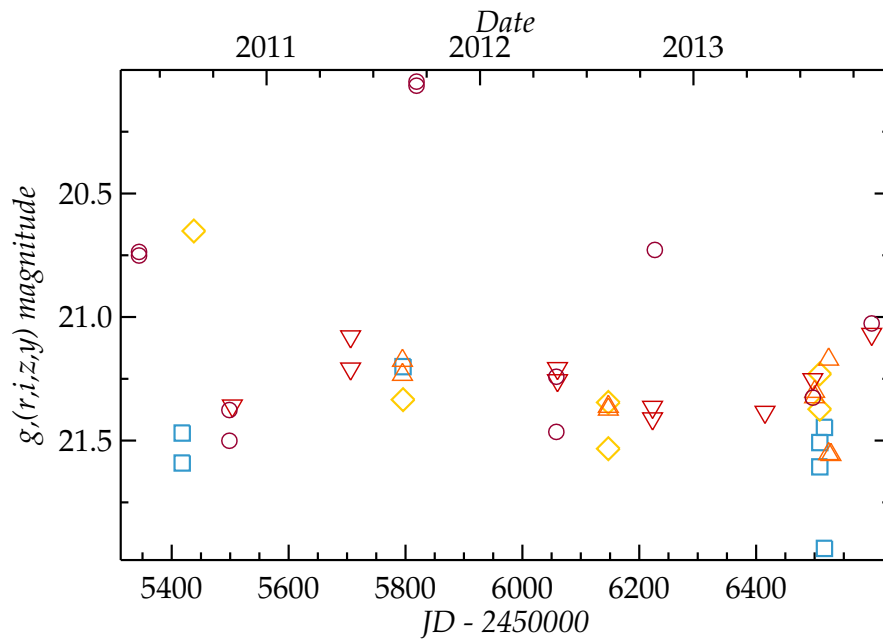


Figure 15: Epoch plot of the Pan-STARRS data of ZTFJ210705.14+394617.7 data with the different bands aligned on the g data as described earlier. Most of the data are in quiescence but a small number of observations have caught the system in outburst. The symbols are as in Figure 3.

3.5 ZTFJ210705.14+394617.7

ZTFJ210705.14+394617.7 has $G = 20.3$ and a companion 0^m5 fainter at 5.6 arcsec. The ZTF data cover four complete observing seasons and show fifteen outbursts with amplitudes of 2–3 magnitudes (see Figure 14). These are well defined with no sign of intermediate, fainter outbursts. The variation at quiescence is 0^m5 – 1 magnitudes but it has no obvious structure. The Pan-STARRS data shown in Figure 15 are mostly at quiescence with a small number of observations in outburst. Details of the best observed outbursts are shown in Figure 16. The top two panels show about 100 days each and both cover two outbursts while the third panel shows three outbursts over 200 days. Although there is some low-level activity at quiescence there are no other weak outbursts. From the outburst timings it is possible to make a good estimate of the mean interval as 78 ± 10 days from the spacings under 100 days as shown in the fourth panel of Figure 16. The pattern of behaviour is consistent with the system being an SS Cyg-type.

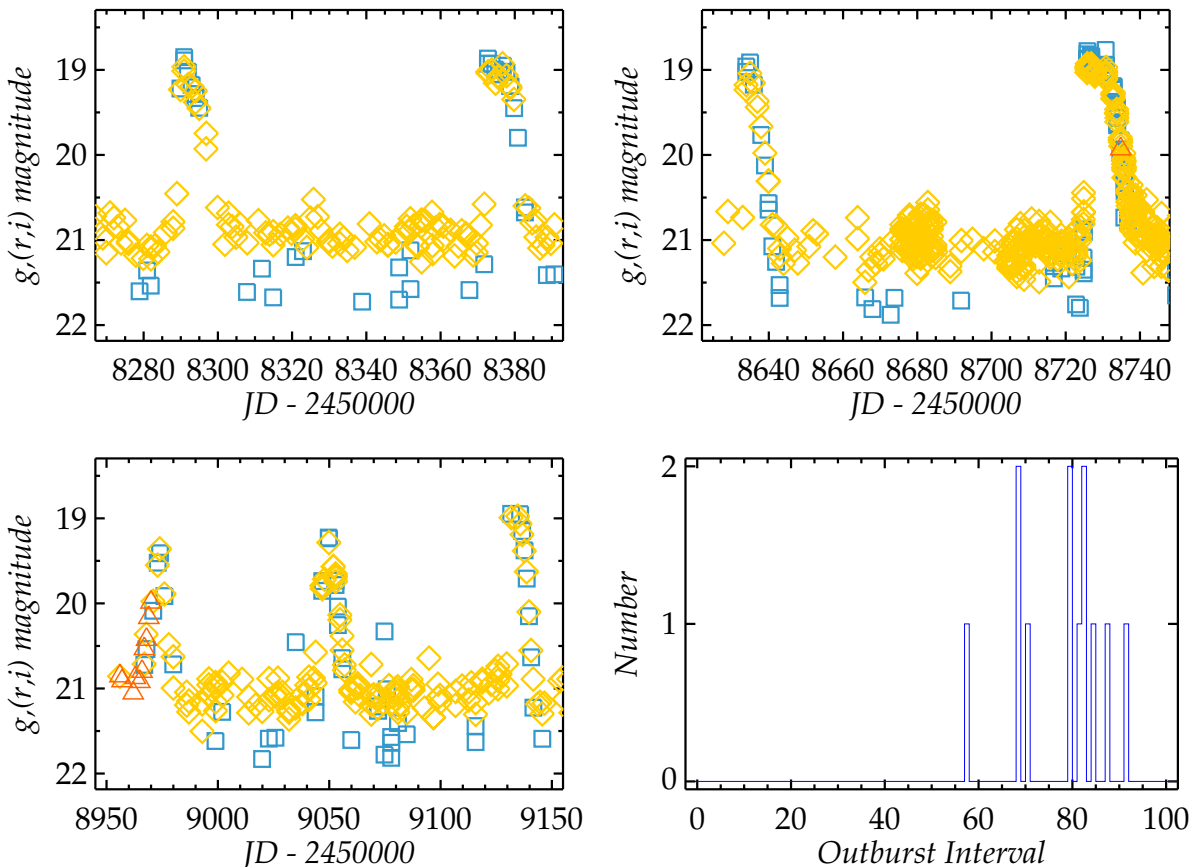


Figure 16: Detail of the ZTFJ210705.14+394617.7 light curve. The top two panels the best coverage over about 100 days each, and the third panel shows about 200 days. The r (diamonds) and i -band data (triangles) are aligned on the g magnitudes (squares) using the bright ($g - r$) offset in Table 1 and the mean ($r - i$) offset. The variation in outburst amplitude and timing is clear, as is the lack of any intermediate outbursts. The fourth panel shows the histogram of the outburst intervals under 100 days.

4 Luminosity and colour

All these systems are faint with $G \sim 20$ so unfortunately the *Gaia* EDR3 parallaxes are poorly determined, and in the case of ZTFJ173854.93+175136.3 not measured. The uncertainties range from about 30–75% which leads to a factor of 2–5 in the measured distances. The *Gaia*-based distance from Bailer-Jones et al. (2021) using the geometric and photo-geometric distance posteriors are also very different, so the uncertainty in the distances, particularly the upper bounds, will feed into the extinction calculation leading to very poorly determined absolute magnitudes.

The colours on the other hand are well determined, particularly when compared with the SDSS snapshot values, but again the uncertainty in the extinction means that they cannot be sensibly dereddened so it is not possible to place these systems on a CV colour-magnitude diagram like *e.g.*, Pala et al. (2020). As dwarf novae evolve to shorter periods the systems become bluer as the cool component and the accretion disc both shrink as the system becomes smaller. However, this is a complex relationship with dependencies on white dwarf mass, accretion rate and other factors. The relationship of the SDSS colours with period has been explored by Szkody et al. (2011) (and earlier papers) and Kato et al. (2012), and in keeping with expectations the short-period SU UMa stars lie at the blue end of the distribution. The short-period systems tend to have $(g - r) \sim 0.0$ and this further supports the conclusion from the light curve that ZTFJ173854.93+175136.3, which has $(g - r) \approx (r - i) = 0.1$, is an SU UMa-type system. It is much bluer than the other systems discussed here which have colours consistent with SS Cyg-type systems.

5 Conclusion

The ZTF Suspected Variables Catalog (Chen et al., 2020) has been searched for new eruptive variables with amplitudes, $\Delta g > 2.0$ magnitudes. The light curves of five stars have been examined and four are likely to be SS Cyg-type systems while the other has the light curve and colours consistent with an SU UMa-type system, and is coincident with a GALEX source.

Acknowledgements: The authors appreciate helpful comments from the referee. The authors are pleased to acknowledge use of NASA’s Astrophysics Data System Bibliographic Services. This research has made use of the SIMBAD database and the VizieR catalogue access tool, CDS, Strasbourg, France (doi.org/10.26093/cds/vizier). This paper made use of the International Variable Star Index (VSX) database, operated at AAVSO, Cambridge, Massachusetts (USA).

References

- Bailer-Jones, C. A. L., Rybizki, J., Foesneau, M., et al., 2021, *AJ*, **161**, 147
 Bellm, E. C., Kulkarni, S. R., Barlow, T., et al., 2019a, *PASP*, **131**, 068003
 Bellm, E. C., Kulkarni, S. R., Graham, M. J., et al., 2019b, *PASP*, **131**, 018002

- Bianchi, L., Herald, J., Efremova, B., et al., 2011, *Ap&SS*, **335**, 161
- Chambers, K. C., Magnier, E. A., Metcalfe, N., et al., 2016, *arXiv e-prints*, arXiv:1612.05560
- Chen, X., Wang, S., Deng, L., et al., 2020, *ApJ Suppl*, **249**, 18
- Coppejans, D. L., K rding, E. G., Knigge, C., et al., 2016, *MNRAS*, **456**, 4441
- F rster, F., Cabrera-Vives, G., Castillo-Navarrete, E., et al., 2021, *AJ*, **161**, 242
- Hellier, C., 2001, *Cataclysmic Variable Stars*, Springer, London
- Kato, T., Isogai, K., Wakamatsu, Y., et al., 2020, *PAS Japan*, **72**, 14
- Kato, T., Maehara, H., & Uemura, M., 2012, *PAS Japan*, **64**, 63
- Masci, F. J., Laher, R. R., Rusholme, B., et al., 2019, *PASP*, **131**, 018003
- Osaki, Y. & Kato, T., 2013, *PAS Japan*, **65**, 50
- Pala, A. F., G nsicke, B. T., Breedt, E., et al., 2020, *MNRAS*, **494**, 3799
- Price, A., Henden, A. A., Foster, G., et al., 2007, *PASP*, **119**, 1361
- Simonsen, M., Boyd, D., Goff, W., et al., 2014, *J AAVSO*, **42**, 177
- Szkody, P., Anderson, S. F., Brooks, K., et al., 2011, *AJ*, **142**, 181
- Warner, B., 1995, *Cataclysmic Variable Stars*, vol. 28 of *Cambridge Astrophysics Series*, CUP, Cambridge